Vision-Guided Autonomous Drones for Search and Rescue (SAR): A Flashing Light Detection Approach

Wei-Chung Chen, Gong-Yi Lee, and Jyi-Shane Liu

***Abstract*—Previously, drones have relied on special markers like H patterns, QR codes, or AprilTags for visual guidance and positioning. While effective for quick positioning, larger marker areas were frequently required at higher altitudes to ensure precise positioning. However, carrying these large markers, especially in emergencies like mountain rescue operations, was impractical for victims. To address this, this study suggests using a flashing light as an alternative solution. Flashing light guidance allows drones to assist rescue personnel in locating and descending near victims to provide clearer environmental information, and land to offer essential supplies when needed. This approach is more convenient than conventional markers and demonstrates practicality during emergencies.**

***Index Terms*—Drone, Flashing Light Detection, Autonomous Landing, Fast Fourier Transform, Human Machine Interaction, Object Detection.**

I. Introduction

RESEARCH on autonomous rescue missions using drones can be divided into three key stages: area search, target localization, and autonomous landing. In the area search stage, drones navigate autonomously to survey disaster-stricken areas quickly [1]. In the target localization stage, they use various sensors and imaging technologies to identify and locate stranded individuals, transmitting real-time information for prompt assistance. The landing stage involves calculating optimal landing points and showcasing autonomous landing capabilities, enabling drones to deliver emergency supplies near stranded individuals. Integrating these stages enhances the efficiency of rescue work efforts by enabling rapid and autonomous rescue operations.

In the past, visual guidance and precise positioning tasks for drones have primarily relied on special artificial markers such as H-shaped patterns [2], QR codes [3], or AprilTags [4]. While these markers are effective, they necessitate a relatively large surface area when used at high altitudes, making them cumbersome and impractical, especially in emergency situations such as mountain rescues. It is unrealistic to expect victims to carry large markers in such scenarios.

In search and rescue missions, many studies have utilized deep learning models to enable drones to detect people from high altitudes [5][6]. However, in practical applications, the wide field of view from a high altitude makes it difficult to confirm whether the detected person is the target of the search and rescue mission. Detection results may include ordinary civilians or rescue teams, necessitating the drone to lower its altitude for ground station personnel to confirm the target. This approach not only wastes drone power but may also delay critical rescue time.

Chen et al. [7] demonstrated that green flashing lights can effectively enhance fire escape efficiency in cinemas. For climbers, it is common to carry a mobile phone with a flashing light or a bicycle flashing light. Therefore, this study proposes the use of a flashing flashlight as an alternative solution, utilizing the blinking light to guide the drone's visual positioning. Compared to traditional markers, a flashing flashlight offers greater adaptability and flexibility. Using a flashlight as a marker requires no additional equipment just a flashlight. Moreover, the flashing light is a distinctive feature that is easily detected and recognized in natural environments. Rescued individuals can guide the drone through the flashing light, facilitating human-machine interaction and assisting the drone in accurately identifying those in need of rescue

This study integrates technologies from various fields to establish a drone system specifically designed for search and rescue operations. Through effective human-machine collaboration, this system enhances the efficiency of search and rescue missions, leading to more successful outcomes. Unlike methods primarily evaluated in simulated environments, we focus on real-world validation through onsite experiments. Our innovative approach replaces traditional markers with flashing lights for target localization, allowing more flexible and efficient search and rescue missions. This expansion of drone applications offers a simpler and more practical alternative, ensuring successful rescue operations across various scenarios. The study aims to enhance drone efficiency and flexibility in disaster missions by integrating technologies and introducing flashing lights.

II. Related Work

A. Flashing light detection

Previous research on light detection [8][9] for recognizing traffic lights in autonomous vehicles focused on color spaces and circular shapes to extract signal candidates. Commonly, traffic light signals have circular and arrow-shaped lights, making the detection of circular objects effective. Yoneda et al. research [10] proposed an alternative algorithm that identifies areas with high luminance and saturation, generating highlighted images. This method estimates the likelihood of illuminated objects, reducing false detections from surrounding illuminated objects. In the context of drones for mountain rescue scenarios, where flashlight styles vary, this approach aligns better with our requirements.

Manuscript received 5 September 2024; revised 2 October 2024; accepted 5 October; Date of publication 17 November 2024.

Wei-Chung Chen, Gong-Yi Lee and Jyi-Shane Liu (Corresponding author) are with the Department of Computer Science, National Chengchi University, Taipei, Taiwan (e-mail: jsliu@cs.nccu.edu.tw).

B. Autonomous landing system

Traditional landing methods heavily rely on the Global Positioning System (GPS), but research [11] has emphasized limitations and risks associated with GPS, such as susceptibility to interference from buildings, terrain, electromagnetic interference, and adverse weather conditions.

This can lead to positioning errors or signal loss. Given the current meter-level accuracy of GPS signals, developing a visual guidance landing mechanism offers a more resilient and precise alternative.

Vision-based autonomous landing for drones provides real-time awareness of changes in the surrounding environment, enhancing landing safety by enabling swift responses to unexpected situations. Xin et al. research [12] synthesized past studies on autonomous drones, categorizing landing sites into static, dynamic, and complex scenes. Static scenes are subdivided into artificial markers and natural landmarks, while dynamic scenes encompass vehicle-mounted and ship-mounted platforms. This study will focus on relevant technologies and applications in static scenes.

The Extended Kalman Filter (EKF) serves as a widely adopted approach in the control system for autonomous drone landing, offering the advantage of integrating sensor information for estimating target position and motion state [13]. This estimation enables real-time motion control, allowing the drone to achieve the landing mission. Another proposed method is staged execution [14], which divides the landing mission into sequential stages, enhancing resilience by organizing tasks based on distance to the target and conducting correction stages to narrow the error range. This approach exhibits stronger resilience compared to previous methods.

III. FLASHING LIGHT DETECTION

This phase of the study lies in the detection of flashing lights with fixed frequency. Drones adhere to pre-designed flight paths, momentarily halting in the air after traversing a specific distance to capture images over a designated time frame. Following this, we isolate regions from each image exhibiting elevated luminance and notable changes, designating them as potential candidate areas for flashing lights. Further analysis is performed on all candidate areas by segmenting the images into multiple sections and concurrently calculating the brightness variations within each area. These variations are then transformed into the frequency domain using the Fourier transform, and the consistency of frequencies within the same area segments is compared.

Upon confirmation of the flashing light, CSRT tracking [15] technology is utilized to match the surrounding area of the flashing light, enabling subsequent flashing light tracking. This method amalgamates multiple aspects such as brightness, variation, and frequency analysis to augment the accuracy and reliability of detecting flashing lights.

A. Detection

For identifying flashing light sources with a fixed frequency. the process is primarily divided into three stages: cumulative image, frequency matching, and final operator confirmation. Compared to other area, the flashing light source area exhibits higher brightness variation. Incorporating attention to the overall change magnitude aids in distinguishing whether the alteration is continuous and stable.

The flowchart depicting the cumulative image stage is demonstrated in Fig. 1.

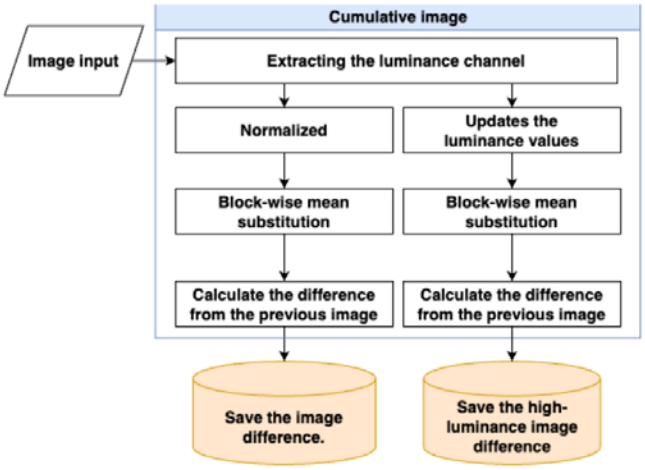

Fig. 1. Flowchart of the cumulative image stage

When the image is received, the luminance channel is extracted, and the luminance values are updated to eliminate background noise. The luminance value is normalized using the following equation:

$$L_m(u,v) = a_l\hat{L} + \frac{\sigma_L}{\sigma}\left(L(u,v) - \hat{L}\right) \tag{1}$$

where $L(u,v)$ and $L_m(u,v)$ represent the original luminance from the HSL image and the modified luminance value at pixel (u,v), respectively. $\hat{L}$ denotes the average luminance of the original luminance image L. σ is the standard deviation for L, and σ_L is the modified standard deviation for the updated image L_m, a_l is a constant parameter that increases the average luminance.

The pixels with luminance lower than this value are reduced using the following equation:

$$L_U(u,v) = L(u,v) * \frac{1}{\left(1+exp\left(-\beta_l(L(u,v)-\gamma_l)\right)\right)} \tag{2}$$

where $L(u,v)$ and $L_U(u,v)$ represent the original luminance from the HSL image and the updated luminance value at pixel (u,v), respectively. β_l and γ_l are constant parameters of the sigmoid function to reduce the luminance value.

Next, we will perform block-based mean replacement operations on $L_m(u,v)$ and $L_U(u,v)$ respectively. Due to the influence of wind on the hovering drone, slight movements may occur in the image. In such scenarios, averaging operations can effectively mitigate the impact of camera shaking and the loss of image stabilization. The calculation is as follows:

$$I_{new}(u,v) = \frac{1}{k^2}\sum_{i=1}^{k}\sum_{j=1}^{k} I(u+i, v+j) \tag{3}$$

where $I_{new}(u,v)$ represents the pixel value at position (u,v) in the replaced image, and $I(u+i, v+j)$ represents the pixel value at position $(u+i, v+j)$ in the original image.

Subtract the previous frame from the current frame, calculate the absolute value, and record these changes. Once a sufficient number of images have been accumulated (set to five

seconds in this study), the system will proceed to the frequency matching stage to verify if the frequency is consistent and continuous. The flowchart depicting the frequency comparison stage is demonstrated in Fig. 2.

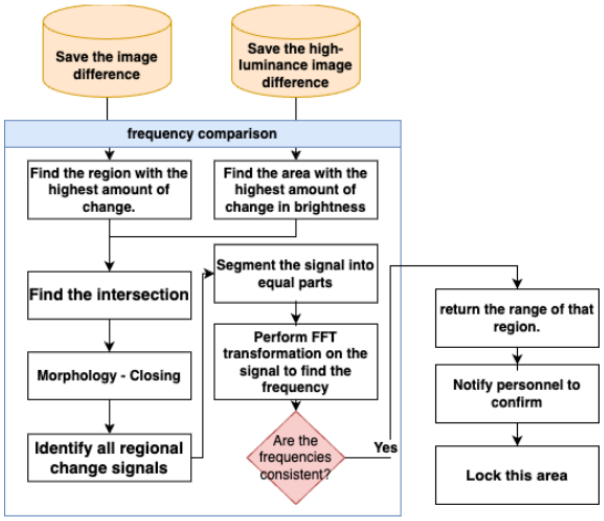

Fig. 2. Flowchart of the frequency comparison stage

Extract information from the previously saved changes and brightness variation. Eq. (4) calculates the sum of all changes. Next, scale the original pixel values to the range of 0 to 255 using linear mapping. Identify the regions with the highest change and the highest brightness variation. Then, determine the intersection of these two regions.

$$I_{total}(u,v) = \sum_{i=1}^{n} I_i(u,v) \tag{4}$$

The Morphology-Closing method is applied to bridge-disconnected but closely located blocks while removing noise. Subsequently, all candidate regions undergo further analysis by segmenting the image into sections and simultaneously computing the brightness variations within each region. These change data are then transformed into the frequency domain using Fourier transformation. Matching is subsequently conducted to assess the consistency of frequencies within the same regions.

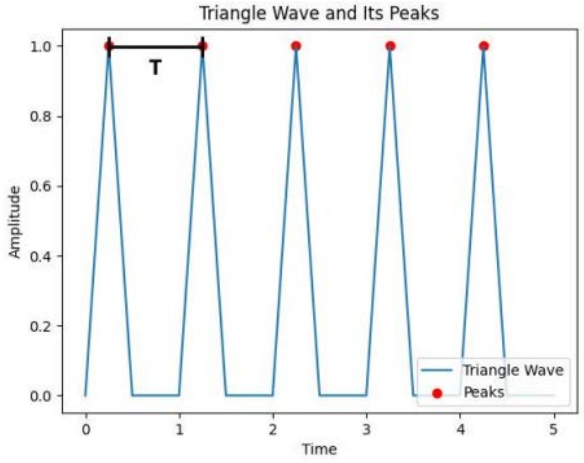

Fig. 3. Triangle Wave and Its Peaks

In the frequency matching stage, the signal variations collected are divided into equal parts, with the video data segmented into 5 equal intervals of 1 second each. The flashing light signals typically exhibit a waveform resembling a triangular wave, characterized by distinct rising and falling edges. Initially, peak detection is performed on the first second of the signal to determine its period and calculate the fundamental frequency. This frequency serves as the baseline for subsequent signal analysis. For triangular waveforms, a common method to estimate the period is by detecting the waveform's peaks, which represent the local maximum points. These peaks are then used to calculate the period and the fundamental frequency, as shown in Fig. 3.

Assume a flashing light signal x, where $x = \{x[n] \mid n = 0, 1, 2, \dots, N-1\}$, with N representing the total number of signal samples. To identify the signal's peaks, we locate the peak points based on changes in the slope. The set of peak indices P is defined by the following condition:

$$P = \{n \mid x[n] > x[n-1] \text{ and } x[n] > x[n+1], n = 1, 2, \dots, N-2\} \tag{5}$$

Using the peak indices P, the time intervals Δt between consecutive peaks can be calculated as:

$$\Delta t = \frac{p[i+1]-p[i]}{f_s}, for\ i = 0, 1, \dots, |P| - 2 \tag{6}$$

where f_s is the sampling rate. Due to the periodic nature of the triangular wave, the period T is derived from the mean of the time intervals between adjacent peaks:

$$T = mean(\Delta t) \tag{7}$$

Finally, the frequency f is calculated as the inverse of the period:

$$f = \frac{1}{T} \tag{8}$$

After determining the fundamental frequency, a Fast Fourier Transform (FFT) is applied to the remaining four segments of the signal. The FFT results are used to filter out frequency components with amplitudes exceeding a predefined threshold, and the frequency closest to the fundamental frequency is selected from these components. This method allows for precise evaluation of signal consistency across different segments and ensures that the FFT results align with expectations from the initial time-domain analysis. The FFT process is as follows: given a signal $x[n]$, where $n = 0, 1, 2, \dots, N-1$, the FFT transforms the signal from the time domain to the frequency domain:

$$Y[k] = \sum_{n=0}^{N-1} x[n] e^{-i2\pi n/N} \tag{9}$$

From the FFT results, the frequency components with amplitudes exceeding a threshold (e.g., 20% of the maximum amplitude) are identified:

$$P = \{k \mid |Y[k]| > 0.2 * max(|Y|)\} \tag{10}$$

Among the identified peak frequencies, the one closest to the expected frequency $f_{expected}$ is found as:

$$f_{closest} = min(|f[P] - f_{expected}|) \tag{11}$$

To account for the wide range of frequencies that may occur in practice, a dynamic threshold based on the expected frequency is set. Given the identified peak $f_{closest}$ and the expected frequency $f_{expected}$, the acceptance condition for this peak is:

$$\left|f_{closest} - f_{expected}\right| < min\left(\zeta_1 * f_{expected},\ \zeta_2\right) \quad (12)$$

Where ζ_1 is the acceptable error ratio, and ζ_2 is the maximum allowable frequency error. In this study, ζ_1 is set to 0.3, and ζ_2 is set to 1.5 Hz. This dynamically adjusted threshold ensures high accuracy in the analysis and guarantees the reliability of the results.

In the drone's actual flight monitoring process, occasional frame drops during video transmission may compromise the integrity of the signal, severely affecting the drone's ability to recognize flashing light sources at a fixed frequency. To address this issue, a sliding window mechanism is introduced in this study. By adding an additional second of recording time to the drone's image collection system, a total of 30 frames are collected. If the frequency matching cannot be completed within the first five seconds of the candidate region, the entire sequence shifts backward by one frame, continuing this process until the additional second of footage is exhausted. This improvement significantly reduces the risk of missing critical targets and enhances the overall reliability of target detection, as illustrated in Fig. 4. This optimization method ensures that more frames are captured during the image collection process. Even if frame drops occur, the sliding window mechanism maintains the drone's ability to effectively identify fixed-frequency flashing light sources. In this way, the drone monitoring system can maintain stable target detection over a wider range, improving the reliability and accuracy of the entire monitoring process.

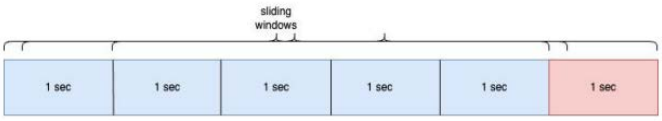

Fig. 4. Sliding windows mechanism.

Upon confirmation that the frequencies segmented from the same candidate block are consistent, the system will annotate and mark that region, alerting the operator for secondary confirmation. Upon verification of the region's accuracy by the operator, a CSRT tracker will be deployed in place for continued flashing light tracking.

The detailed visualization of the image processing process is depicted in Fig. 5. (a) shows the search for the region with the highest amount of change, (b) identifies the region with the highest amount of change in brightness, and (c) find the intersection regions from (a) and (b). In the figure, these intersecting regions are represented by several bright spots, such as a series of bright points in the upper-left corner, a bright point in the center, and other scattered bright points near the edges. Finally, (d) illustrates the result after applying Morphology-Closing, FFT, and frequency matching. The system confirms that the frequency in the central bright spot is consistent and returns this region, which is highlighted with a green box.

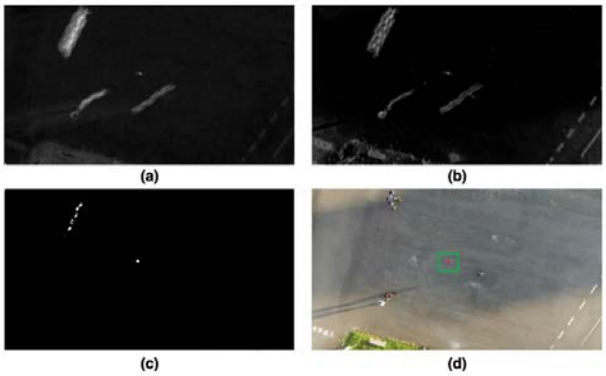

Fig. 5. Image processing results in detecting flashing light.
(a) The region with the highest amount of change.
(b) The region with the highest amount of change in brightness.
(c) Find the intersection from (a) and (b).
(d) After frequency matching, the system returns the detected region.

B. Tracking

CSRT (Channel and Spatial Reliability Tracker) is an object-tracking algorithm that improves performance by integrating information from both channel and spatial reliability. It utilizes target features across various channels and considers spatial correlation for enhanced tracking stability and precision.

In a previous study by Brdjanin et al. [16], benchmark tests were conducted on the OTB-100 dataset, evaluating eight trackers available in the OpenCV library. The research used two evaluation methods, OPE and SRE, along with Precision and Success Plot, to assess the robustness of each algorithm. The results indicated that the CSRT tracker exhibited the most favorable overall performance in terms of accuracy and Intersection over Union (IoU) rate.

Based on prior research, we have selected the CSRT tracker to achieve real-time flashing detection and tracking during the descending flight step of the drone. Its efficiency and stability enable swift adaptation to changes in the target's position in dynamic environments, ensuring continuous tracking. This real-time detection and tracking capability is pivotal for the drone landing operation, assisting us in precisely tracking the flashing light and accomplishing the mission. The benefit of the CSRT tracker excels in understanding target features and spatial relationships, adapting seamlessly to changes in lighting, wind speed, and target size for accurate and stable tracking.

IV. VICTIM VERIFICATION

The victim verification phase comprises three steps: flashing light confirmation, descending flight, and ground image capturing, represented by nodes in the Behavior Tree [17]. Initially, at high altitudes, the drone aligns and corrects its position using flashing light information from image feedback. The drone then descends, continuously monitoring the environment below through real-time imaging and sensing technologies, and adjusts its position continuously to ensure that the flashing light remains centered. Upon reaching a lower altitude, it enters the image collection step, rotating counterclockwise to capture clear low-altitude image data for the operator to confirm and decide whether to land. The corresponding Behavior Tree is demonstrated in Fig. 6.

In the flashing light confirmation steps, the drone hovers at

a high altitude until it determines the flashing light coordinates in the image. If the flashing light is lost, the drone remains hovering to prevent loss of control. After obtaining the flashing light coordinates, the Behavior Tree checks if the current altitude exceeds the preset height k meters. If it does, the drone enters the ground image.

During the descending flight step, the system calculates the horizontal error d_x and vertical error d_y between the flashing light coordinates t and the center point c of the screen, as shown in Eq. (13):

$$d_x = t_x - c_x, d_y = t_y - c_y \tag{13}$$

Where t_x and t_y represent the horizontal and vertical positions of the flashing light in the screen coordinates, and c_x and c_y represent the horizontal and vertical positions of the screen center point.

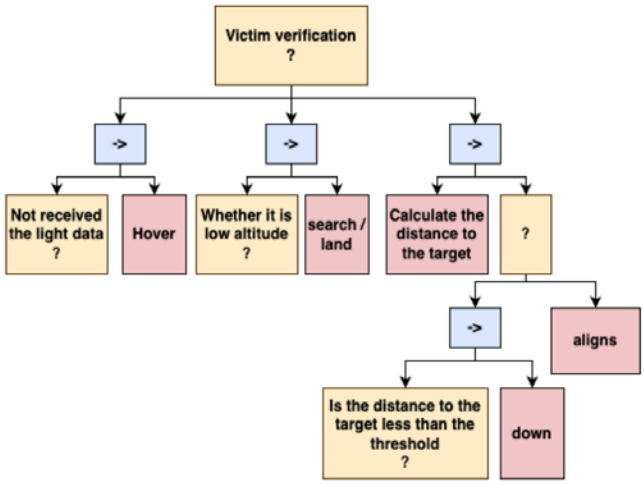

Fig. 6. A Behavior Tree for victim verification task.

If either d_x or d_y exceeds a predefined threshold (set to 2 meters in this study), Eq. (14) will be utilized to compute the drone's motion commands for alignment. If the distance is below the threshold, the drone will initiate a descent maneuver, setting Δz to -1, with a velocity of approximately 1 meter per second, ultimately accomplishing the entire autonomous landing task.

$$\Delta x = \frac{-d_x}{|d_x|} * \theta_1, \Delta y = \frac{d_y}{|d_y|} * \theta_2, \Delta z = 0 \tag{14}$$

Δx denotes the horizontal movement speed of the drone, Δy signifies the forward and backward movement speed of the drone, and Δz represents the descent speed. During the correction process, Δz is set to 0 to indicate a pause in descent. θ_1 and θ_2 are adjustable variables employed to regulate the speed, configured to 0.15 and 0.2, approximately 0.15 meters per second and 0.2 meters per second, respectively.

Once the drone descends to a lower altitude (set at 4 meters above ground level in this study), it can commence capturing images of the surrounding area to evaluate the situation of the victim. The drone will rotate counterclockwise in place, gathering image data, and utilize YOLOv8 [18] for human identification. After identification is completed, the image data will be transmitted back for the operator to confirm the necessity for landing.

V. HUMAN-MACHINE INTERACTION INTERFACE

Fig. 7. illustrates the ground station human-machine interaction interface during an actual flight in the experimental environment. The interface is divided into an upper and a lower part. The left side of the upper part displays the real-time live feed from the flight, while the middle section shows the image after target positioning, with a green box indicating the target area, a blue dot representing the center of the area, and a red box indicating the drone's center field of view. The mission objective is to align the blue dot within the red box area. The right side displays the current status information of the drone, including battery level, flight altitude, flight speed, GPS coordinates, and frames per second (fps).

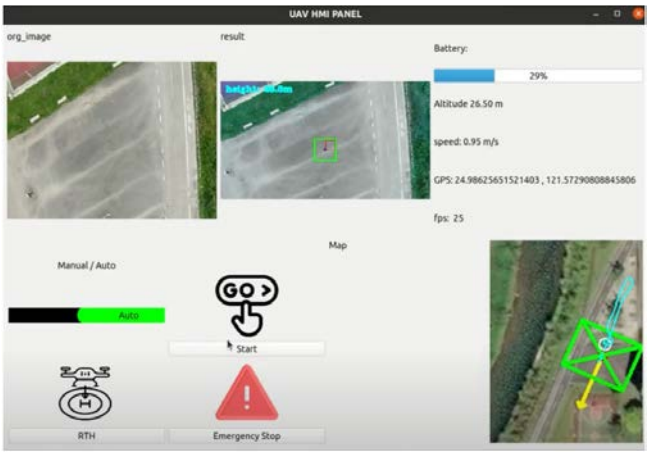

Fig. 7. UAV HMI Panel

The left side of the lower part contains functional buttons for sending control commands to the drone. These buttons include toggles for automatic and manual control, takeoff start, Return to Home (RTH), and emergency stop. In automatic control mode, pressing the start button will trigger the drone to take off and execute the mission; in an emergency, pressing the emergency stop button will cause the drone to halt its current action and hover in place. Afterward, the RTH button can be pressed to make the drone return home autonomously, or it can be switched to manual control for the operator to take over.

VI. EXPERIMENTAL RESULTS

This study presents SAR (Search and Rescue) applications utilizing an autonomous navigation control system that incorporates flashing light detection, implemented on a DJI Mavic 2 Zoom micro UAV. The control system is run by the ROS (Robot Operating System) on a notebook computer with AMD5900 CPU processor, RTX3070 video card, and 16GB memory. The data connection between the notebook computer and the DJI Mavic 2 Zoom is via its remote controller and a cell phone.

A. Experiment Design

- Verification in different scenarios:

This study selected four different locations to conduct drone flashing light verification experiments to ensure the generalizability and representativeness of the experimental results. The experiments included six different scenarios, as shown in the Fig. 8. An ELOPS 300-lumen LED bicycle front

light was used as the light source in the experiments, and the drone's flight altitude was set at 20 meters.

In each scenario, we recorded a 10-second video, totaling 300 frames. The first 5 seconds (150 frames) of footage were used to determine whether the flashing light source was detected in the next frame and to calculate the hit rate for that footage. All frames contained the flashing light source, so the hit rate was calculated as follows:

$$\text{Hit Rate} = \frac{Number\ of\ correctly\ identified\ frames}{Total\ number\ of\ identified\ frames} \quad (7)$$

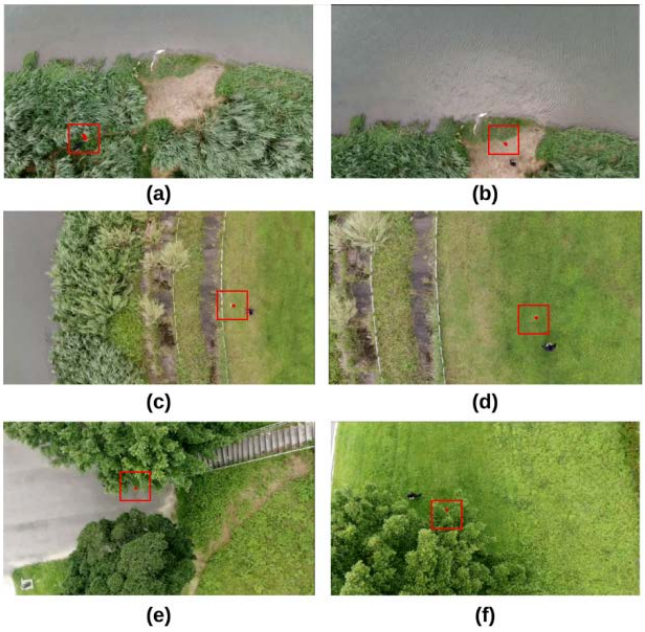

Fig. 8. Flashing light detection in different scenarios.

Fig. 8. illustrates various scenarios tested to evaluate the effectiveness of flashing light detection in different environments. In Fig. 8 (a), the scenario took place on sand dunes beside a river, with the light source positioned on a fern-covered path leading into the dunes. This setup primarily tested the detection effectiveness when the light source was obscured by fern plants. In Fig. 8 (b), within the same location as Fig. 8 (a), the light source was positioned on the path, focusing on whether reflections from the river's surface affected the detection of the flashing light. Moving to Fig. 8(c), the scenario was set on a grassy area on the riverbank, with the light source positioned on the grass, testing the influence of river reflections on detection. In Fig. 8(d), still on the grassy riverbank, the light source's detection effectiveness was assessed without the interference of river reflections. Fig. 8(e) presented a scenario between two trees, with the light source positioned under them, testing detection effectiveness under the tree. Finally, Fig. 8(f) examined detection effectiveness under the shadow of a single tree, with the light source positioned beneath it.

- Verification of different flashing light frequencies:

In this experiment, our aim is to validate the applicability of the flashing light detection system to different frequencies of fixed flashing lights. To achieve this, we will use the iPhone 13 rear flashlight to generate flashing light sources with frequencies of 5, 10, 13, and 15 Hz, respectively, and place them on the ground. The drone will conduct tests at a flight altitude of 10 meters to simulate real-world scenarios. Through this design, we can comprehensively evaluate the system's detection performance for flashing light sources at different frequencies, thereby enhancing its reliability and practicality across various application scenarios.

- Complete search and rescue experiment:

We selected two areas near the campus for our experiments. The first experimental area is Daonan Riverside Park, located near the river. The second experimental area is situated in the mountainous region at the NCCU Research, Innovation, and Incubation Center. We thoroughly tested the search and rescue system proposed in this experiment, which includes the detection of flashing lights and the autonomous descent of the drone followed by a stationary counterclockwise rotation to search for and recognize individuals in the imagery.

B. Experiment Results

Since flashing lights are difficult to represent in still images, we have provided a video of our experimental results, available on YouTube at the following link: https://www.youtube.com/watch?v=XOFvYqqXqmk.

- Verification of different scenarios:

In our experimental video, the results of the "Verification of different scenarios" are shown from the 3rd second to the 38th second. Under the validation of our scenarios, there were no false positives observed. The performance in scenarios (a) ~ (d) was satisfactory, with hit rates exceeding 80%. However, in scenarios (e) and (f), occasional gusts of wind causing tree branches to completely obstruct the light source disrupted the flashing signal, resulting in lower hit rates.

TABLE I

RESULTS OF FLASHING LIGHT DETECTION IN DIFFERENT SCENARIOS

	Hit Rate		**Hit Rate**
Scenario (a)	82.29 %	**Scenario (d)**	85.14 %
Scenario (b)	85.71 %	**Scenario (e)**	40.83 %
Scenario (c)	89.22 %	**Scenario (f)**	46.43 %

- Verification of different flashing light frequencies:

In our experimental video, the results of the "Verification of different flashing light frequencies" are shown from the 39th second to the 1st minute and 4th second. Fig. 9. shows the scenarios of our experiments with different frequencies of flashing lights, including 5 Hz, 10 Hz, 13 Hz, and 15 Hz, while Fig. 10. displays the signals of the flashing lights at different frequencies and their waveforms after Fourier transformation. The experimental results indicate that flashing light signals with frequencies of 5 Hz, 10 Hz, and 13 Hz were successfully recognized. However, the flashing light signal with a frequency of 15 Hz was not successfully recognized. This is because the frame rate (fps) of the images collected by the drone is 30, and we performed signal analysis on a per-second basis. According to the sampling theorem, our maximum sampling frequency is 30/2, which is 15 Hz. Therefore, the actual

maximum frequency that can be sampled should be (30/2) - 1, which is 14 Hz, making the 15 Hz signal beyond the recognizable range.

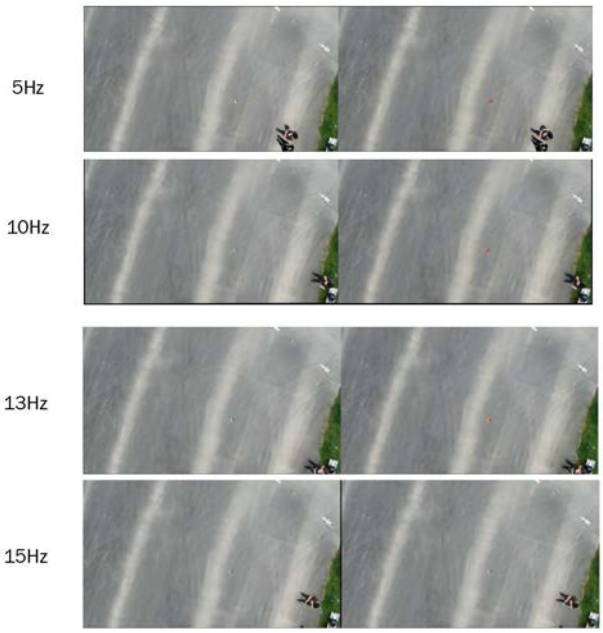

Fig. 9. Different frequency verification scenarios.

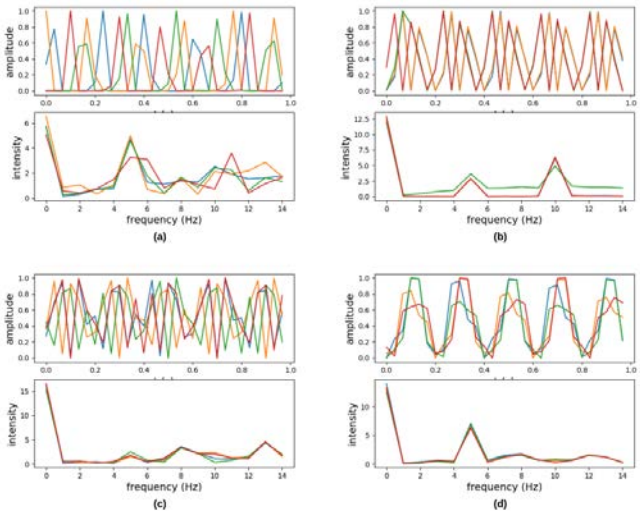

Fig. 10. Flashing lights at different frequencies.

(a) 5hz, (b) 10hz, (c) 13hz, (d) 15hz.

- Complete search and rescue experiment:

From Fig. 11., it can be observed that our flashing light detection system exhibits excellent applicability across various environments. The system functions effectively in settings such as wilderness or suburban areas, making it adaptable to different search and rescue scenarios. This holds significant importance in enhancing the efficiency and success rate of rescue operations.

From Fig. 12., it is evident that the drone guided by flashing lights successfully descends autonomously to the preset appropriate altitude for capturing higher resolution images. Subsequently, through counterclockwise rotation, clearer image data is obtained. We have successfully utilized YOLOv8 to identify individuals in need of rescue. These image data are then transmitted back to the operator to assist in subsequent rescue operations. This outcome demonstrates the reliability of our system across different environments, providing substantial support and assistance for search and rescue missions.

Fig. 11. Flashing light in different environments.
(a) Areas for the first experiment. (b) Areas for the second experiment.

Fig. 12. Victim detection in different environments.
(a) Victim detection on first experiment.
(b) Victim detection on second experiment.

VII. Conclusion

This study presents a human-machine collaboration system designed for Search and Rescue (SAR) applications utilizing drones. Our system utilizes flashing light sources instead of traditional markers, enabling drones to accurately descend to the vicinity of trapped individuals and collect clearer image data to provide rescue personnel with more comprehensive information, and land to deliver emergency supplies when necessary. Real-world validations showcase the efficacy of our system across diverse scenarios. In addition to testing with the iPhone's flashing light, we conducted experiments using an ELOPS 300-lumen LED bicycle front light, further demonstrating the system's capability to detect and respond to various light sources. Moving forward, we aim to enhance the system's robustness by extending its detection capabilities beyond fixed frequency patterns, allowing it to reliably identify other human-generated signals such as hand waves, moving tree branches, or even torches.

To further enhance the robustness and applicability of the system, we plan to conduct comprehensive validations under various environmental conditions, including nighttime and foggy weather. We will also evaluate its performance with different types of light sources, particularly in scenarios where the light source may be in motion. Additionally, further development of simulation methods will ensure a thorough and precise evaluation of our approach.

In summary, while this study has made significant contributions to SAR applications using drones, addressing these areas of improvement will future refine and expand the

system's capabilities. Future endeavors will also explore additional application domains, including logistics delivery or inspection tasks.

REFERENCES

[1] S. Yuan, K. Ota, M. Dong, and J. Zhao, "A path planning method with perception optimization based on sky scanning for UAVs," Sensors, vol. 22, no. 3, p. 891, Jan. 2022.
[2] Y. Jung, D. Lee, and H. Bang, "Close-range vision navigation and guidance for rotary uav autonomous landing," in 2015 IEEE International Conference on Automation Science and Engineering (CASE). IEEE, pp. 342–347, 2015.
[3] T. W. Kang, and J. W. Jung, "A Drone's 3D Localization and Load Mapping Based on QR Codes for Load Management," Drones, vol. 8, no. 4, p. 130, Mar. 2024.
[4] S. Kyristsis, A. Antonopoulos, T. Chanialakis, E. Stefanakis, C. Linardos, A. Tripolitsiotis, and P. Partsinevelos, "Towards Autonomous Modular UAV Missions: The Detection, Geo-Location and Landing Paradigm," Sensors, vol. 16, no. 11, p. 1844, Nov. 2016.
[5] M. Bejiga, A. Zeggada, A. Nouffidj, and F. Melgani, ''A convolutional neural network approach for assisting avalanche search and rescue operations with UAV imagery,'' Remote Sens., vol. 9, no. 2, p. 100, Jan. 2017.
[6] I. Martinez-Alpiste, G. Golcarenarenji, Q. Wang, and J. M. Alcaraz-Calero, "Search and rescue operation using UAVs: A case study," Expert Syst. Appl., vol. 178, Sep. 2021, Art. no. 114937.
[7] Z. Chen, P. Han, Z. He, Z. Yang and Y. Liang, "Enhancing Cinema Evacuation Efficiency: Impact of Flashing Lights on Emergency Egress Performance and Fire Safety," in IEEE Access.
[8] Y. Lu, J. Lu, S. Zhang, and P. Hall, ''Traffic signal detection and classification in street views using an attention model,'' Comput. Vis. Media, vol. 4, no. 3, pp. 253–266, Sep. 2018.
[9] J.-G. Wang and L.-B. Zhou, "Traffic light recognition with high dynamic range imaging and deep learning," IEEE Trans. Intell. Transp. Syst., vol. 20, no. 4, pp. 1341–1352, Apr. 2019.
[10] K. Yoneda, A. Kuramoto, N. Suganuma, T. Asaka, M. Aldibaja, and R. Yanase, "Robust traffic light and arrow detection using digital map with spatial prior information for automated driving," Sensors, vol. 20, no. 4, Feb. 2020, Art. no. 1181.
[11] S. Z. Khan, M. Mohsin, and W. Iqbal, "On GPS spoofing of aerial platforms: A review of threats, challenges, methodologies, and future research directions," PeerJ Comput. Sci., vol. 7, May. 2021, Art. no. e507.
[12] L. Xin, Z. Tang, W. Gai, and H. Liu, ''Vision-based autonomous landing for the UAV: A review,'' Aerospace, vol. 9, no. 11, p. 634, Oct. 2022.
[13] M. Y. Arafat, M. M. Alam, and S. Moh, ''Vision-based navigation techniques for unmanned aerial vehicles: Review and challenges,'' Drones, vol. 7, no. 2, p. 89, Jan. 2023.
[14] S. Lin, L. Jin, and Z. Chen, ''Real-time monocular vision system for UAV autonomous landing in outdoor low-illumination environments,'' Sensors, vol. 21, no. 18, p. 6226, Sep. 2021.
[15] K. Farkhodov, S.-H. Lee, and K.-R. Kwon, "Object tracking using csrt tracker and rcnn." in BIOIMAGING, pp. 209–212, 2020.
[16] A. Brdjanin, N. Dardagan, D. Dzigal, and A. Akagic, "Single object trackers in OpenCV: A benchmark," in 2020 International Conference on INnovations in Intelligent SysTems and Applications (INISTA). IEEE, Aug. 2020.
[17] M. Iovino, E. Scukins, J. Styrud, P. Ögren, and C. Smith, "A survey of behavior trees in robotics and AI," Robot. Auton. Syst., vol. 154, 2022, Art. no. 104096.
[18] M. Rizk and I. Bayad, "Human Detection in Thermal Images Using YOLOv8 for Search and Rescue Missions," in 2023 Seventh International Conference on Advances in Biomedical Engineering (ICABME), pp. 210–215, 2023.

Wei-Chung Chen received the M.S. degree in Department of Computer Science from National Chengchi University, Taipei, Taiwan, in 2024. He is currently a Technology Management Associate with the E.SUN Bank, Taiwan. His current research interests and publications are in the areas of Robot System, Artificial Intelligence, Algorithm Application and Software Coding.

Gong-Yi Lee received the M.S. degree in Department of Computer Science from National Chengchi University, Taipei, Taiwan, in 2019. He is currently Ph.D. student in Department of Computer Science from National Chengchi University, Taipei, Taiwan. His current research interests and publications are in the areas of Robot System, Autonomous Decision Making, Artificial Intelligence, Algorithm Application, Software System Integration and Image Process.

Jyi-Shane Liu received the M.S. degree in Mechanical Engineering from The State University of New York at Stony Brook, New York City, United States and both M.S. and Ph.D. degree in Robotics Institute from Carnegie Mellon University, Pennsylvania, United States. He is currently the Dean of the College of Informatics at National Chengchi University, Taipei, Taiwan. His current research interests and publications are in the areas of Artificial Intelligence, Robotics, Intelligent Drones, Digital Humanities, Social Network Analysis, Digital Library.